# Emergent dynamic structures and statistical law in spherical lattice gas automata

Zhenwei Yao*

*School of Physics and Astronomy, and Institute of Natural Sciences, Shanghai Jiao Tong University, Shanghai 200240, China*

(Received 13 August 2017; revised manuscript received 5 October 2017; published 26 December 2017)

Various lattice gas automata have been proposed in the past decades to simulate physics and address a host of problems on collective dynamics arising in diverse fields. In this work, we employ the lattice gas model defined on the sphere to investigate the curvature-driven dynamic structures and analyze the statistical behaviors in equilibrium. Under the simple propagation and collision rules, we show that the uniform collective movement of the particles on the sphere is geometrically frustrated, leading to several nonequilibrium dynamic structures not found in the planar lattice, such as the emergent bubble and vortex structures. With the accumulation of the collision effect, the system ultimately reaches equilibrium in the sense that the distribution of the coarse-grained speed approaches the two-dimensional Maxwell-Boltzmann distribution despite the population fluctuations in the coarse-grained cells. The emergent regularity in the statistical behavior of the system is rationalized by mapping our system to a generalized random walk model. This work demonstrates the capability of the spherical lattice gas automaton in revealing the lattice-guided dynamic structures and simulating the equilibrium physics. It suggests the promising possibility of using lattice gas automata defined on various curved surfaces to explore geometrically driven nonequilibrium physics.

DOI: 10.1103/PhysRevE.96.062139

## I. INTRODUCTION

Lattice gas models are powerful and flexible tools to address a host of fundamental problems arising in equilibrium and nonequilibrium statistical physics [1–7], hydrodynamics [8–15], pattern formation [16–21], and dynamical systems [22–25]. Tracking the evolution of many identical agents under a few prescribed rules in computer programs, i.e., the idea of cellular automata [7,26–28], represents an alternative to, rather than an approximation of, differential equations in modeling the natural world [28–30]. A major goal of physics is to build the bridge between a microscopic (level 1) and a macroscopic (level 2) description of reality [4,31]. To this end, various lattice gas automaton models have been proposed. At level 1, the particles follow a few well-defined rules and hop over the lattice. One obtains level 2 phenomena by coarse-graining concerned physical quantities like velocity and particle number. The first fully deterministic lattice gas model, which was defined on the square lattice known as the HPP model, was proposed by Hardy, de Pazzis, and Pomeau to simulate flow phenomena [8,9]. Its variant version FHP model for the triangular lattice was later introduced by Frisch, Hasslacher, and Pomeau [11,12]. These lattice gas models are able to simulate the Navier-Stokes equation in the regime of incompressible fluid [11,12], and reproduce featured flow behaviors in real fluids like vortices and wave propagation [3,10]. For the simplicity of the rules and the capability of simulating physics, these lattice gas models are reliable tools for establishing the connection between the two levels of reality.

We generalize the FHP model to the spherical lattice, and explore the emergent dynamic structures and equilibrium properties at level 2 arising from the microscopic motion of many identical constituents. Here, the spherical lattice refers to a two-dimensional triangular lattice that covers the entire sphere. We choose the spherical lattice based on the following considerations. First, extensive studies in the community of active matter physics have shown that curvature can create rich dynamic structures not found in the planar geometry [32–34]. The spherical lattice is naturally curved, and provides an ideal environment to explore the lattice-guided nonequilibrium dynamic structures. In addition, due to the compactness of the spherical geometry, the subtle influence of the boundary condition can be avoided. In our model, the particles hop over the lattice according to a few well-defined collision and propagation rules. In short, the particles propagate along the lattice unless two particles of opposite velocities occupy the same vertex or three particles move into the same vertex whose total velocity is zero; binary and triple collisions occur in these cases.

In this work, we first show that any orbit of a single particle over the spherical lattice, regardless of its initial position and velocity, is closed and has the identical period. Consequently, a cluster of particles with quasi-uniform initial velocity is observed to separate and merge as a whole with the alternating convergence and divergence of the lattice. In addition to the periodic global morphological transformations, we also discover featured nonequilibrium dynamic modes, including deforming bubbles in their propagation, and localized vortex structures. The presence of the disclinations in the spherical lattice, in combination with the compactness of the spherical geometry, is responsible for all these emergent dynamic structures. The accumulation of the collision effect ultimately brings the system in equilibrium, which is signified by the convergence of the collision frequency curves. Statistical analysis reveals that the number of particles in each coarse-grained cell is subject to the Gaussian-type fluctuation. For modest population fluctuation in the coarse-grained cells, the coarse-grained speed still conforms to the two-dimensional Maxwell-Boltzmann distribution. These results are well rationalized by mapping our system to a generalized random walk model. We further discuss the collision-driven randomization of the coarse-grained particle velocity, by which the application of the random walk model to our system is well justified.

*zyao@sjtu.edu.cn

 

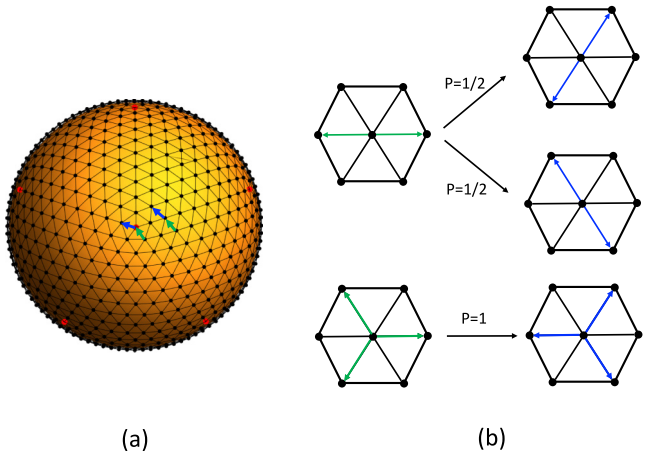


FIG. 1. Illustration of the generalized FHP lattice gas automaton model on the sphere. (a) A spherical lattice where the red dots represent the five-fold disclinations with five nearest neighbors. There are 12 five-fold disclinations over the entire spherical lattice as a topological requirement. The green and blue arrows are to explain the propagation rule on a regular and disclinational vertex. (b) The rules for the head-on binary and triple collisions.

Simulations show that either binary or triple collisions between particles, even at a rate as low as 0.06%, is sufficient to produce the Maxwell-Boltzmann distribution. This work demonstrates that the spherical lattice gas automaton is capable of simulating the geometrically driven nonequilibrium structures and the geometry-independent equilibrium properties. Our model may be generalized to other curved surfaces as well as the almost-planar lattices with a designed mix of five- and seven-fold disclinations to explore the geometrically driven nonequilibrium physics.

## II. MODEL

We generalize the FHP model to the spherical lattice to study the particle dynamics over the sphere. The FHP model was originally designed on the planar triangular lattice. By generalizing it to the spherical lattice, the model is modified accordingly. In the spherical lattice, the point crystallographic defects called disclinations are inevitable [35]. An $n$-fold disclination in a triangular lattice refers to a vertex whose coordination number $n$ is deviated from six. According to the Euler's theorem [37], the total topological charge in a triangular lattice is a topological invariant:

$$\sum_{i\in V} q_i = 6\chi, \tag{1}$$

where $q_i = 6 - z_i$ is the topological charge of the vertex $i$, $z_i$ is the coordination number of the vertex $i$, the sum is over all the vertices $V$ in the spherical lattice, and $\chi$ is the Euler's characteristic. For the spherical topology, $\chi = 2$. It indicates that the total topological charge in the spherical lattice is 12. The presence of the disclinations therein is therefore a topological requirement. The simplest spherical lattice contains uniformly distributed 12 five-fold disclinations. We adopt such a spherical lattice in our work. The red dots in Fig. 1(a) represent the five-fold disclinations. In the original FHP model, each vertex accommodates up to six particles. In the spherical lattice, each five-fold disclination can accommodate up to five particles. The exclusion rule in the original FHP model is inherited in our model. That is, a vertex cannot accommodate two or more particles of the same velocity.

In our model, the states of the particles are simultaneously updated by the following collision and propagation rules. There are two types of collisions: the head-on binary and triple collisions. The head-on binary collision occurs when a vertex is only occupied by two particles of opposite velocities. In a triple collision, three particles meet at the same vertex whose total velocity is zero. The updated particle states after the two kinds of collisions are shown in Fig. 1(b). For the head-on binary collision, the two final states occur with equal probability. The propagation rule is straightforward for a planar triangular lattice: a particle moves along the lattice by the direction of its velocity as shown in Fig. 1(a). On a spherical lattice, all of the particles must turn either left or right uniformly when passing through the disclinations to obey the exclusion rule. Without loss of generality, we require any particle passing a disclination to turn left, as shown in Fig. 1(a). Otherwise, two velocity vectors pointing to a disclination may merge to a single velocity vector after a time step if one of them turns left and the other turns right, which violates the exclusion rule.

Here we note that in the planar FHP lattice gas model, the momentum of the system is conserved in both propagation and collision operations. However, by generalizing the model to the spherical lattice, the direction of a velocity vector is changed in its propagation, which requires a force on the particle. Furthermore, the bonds in the spherical lattice are generally not of the same length except the special case of the icosahedron. Consequently, the total momentum of two or three particles changes slightly after the binary or triple collision. Therefore, unlike that on a planar lattice, an energy input is required to realize the propagation and collision of the particles on the sphere. Such a system may be realized in a group of active agents confined on the sphere [33].

We employ the Casper and Klug scheme to construct the spherical lattice as shown in Fig. 1(a) [36]. Starting from a regular icosahedron with 12 vertices, we introduce $n-1$ points evenly on each edge to divide each face into a number of triangles. The total number of vertices in the resulting spherical lattice is $N = 10n^2 + 2$. To perform the coarse-graining procedure, we introduce another set of triangular lattice on the sphere with the Casper and Klug scheme, and name it the coarse-grained lattice. The sphere is therefore equipped with two sets of lattices: the original lattice where the particles live, and the auxiliary coarse-grained lattice for calculating the coarse-grained quantities. The coarse-grained lattice consists of $N_{cg}$ vertices and $2N_{cg}$ faces, each face containing $N/(2N_{cg})$ vertices in the original spherical lattice. Summing over all the velocity vectors within a triangular face in the coarse-grained lattice gives rise to the associated coarse-grained velocity.

## III. RESULTS AND DISCUSSION

We first consider the motion of a single particle on the spherical lattice. We map the spherical lattice in the three-dimensional Euclidean space to the plane of the spherical

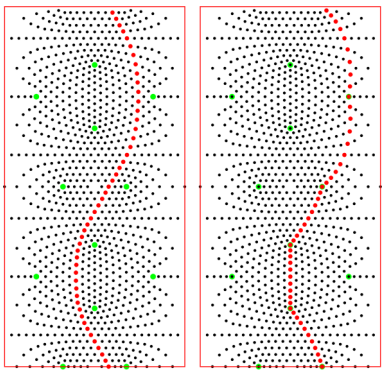


FIG. 2. Closed orbits (in red dots) of a single particle with different initial velocity directions on the spherical lattice plotted in the spherical coordinates. All the orbits of the particle with varying initial velocity directions are closed and have the same period. The horizontal and vertical axes are for $\theta$ and $\phi$, respectively. The green dots represent the five-fold disclinations. $N = 1002$.

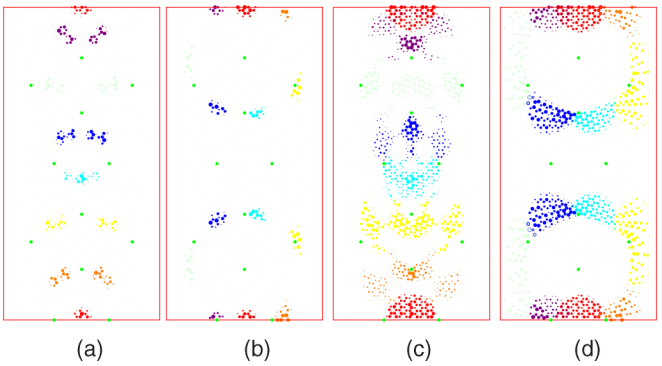


FIG. 3. Periodic separation and merging of the moving clusters. The morphologies of the cluster at different time steps are shown in different colors: from below to above, $t = 1$ (red), 30 (orange), 60 (yellow), 90 (cyan), 120 (light green), and 180 (purple). The size of the colored dots indicates the number of particles in the coarse-grained cells. The green dots represent the disclinations in the original spherical lattice. The sizes of the clusters are (a,c) $r_c = 0.2R$ and (b,d) $0.5R$. $N = 16\,002$. $N_{cg} = 1002$.

coordinates $\{\theta,\phi\}$. $\theta \in [0,\pi]$. $\phi \in [0,2\pi)$. In the rectangular box in Fig. 2, the short and long sides are the axes of $\theta$ and $\phi$, respectively. The black dots are the vertices in the spherical lattice, and the green dots represent the 12 five-fold disclinations. The trajectory of the single particle is shown in red dots. We see that the trajectory is always closed whether the particle passes through a disclination or not. In particular, if the particle passes through a disclination, as shown in Fig. 2(b), it also passes through other four disclinations, forming a closed loop over the sphere. We notice that the period of any closed orbit is the same regardless of the initial position and velocity of the particle.

The combination of the identical period of the closed orbit and the spherical geometry may lead to the periodic morphological transformation of a collectively moving cluster of particles. We create a moving cluster of particles on the spherical lattice to test this conjecture. We first select all the vertices in the spherical lattice whose distance from any reference vertex is smaller than $r_c$, and then put particles on these vertices. The initial velocity of these particles is along one of the six (or five, if a particle sits at a disclination) discrete directions that makes the minimum angle with either the local $\hat{e}_\phi$ or $\hat{e}_\theta$ directions. Thus the cluster is equipped with a quasi-uniform velocity distribution. The evolutions of typical clusters along $\hat{e}_\phi$ and $\hat{e}_\theta$ are shown in Fig. 3. For visual convenience, we work in the coarse-grained lattice; the size of the colored dots indicates the number of particles in each coarse-grained cell. The tempospatial patterns of the clusters are shown by different colors from red at $t = 1$ [see the lower parts in Fig. 3] to purple at $t = 180$ [at the top in Fig. 3]. A salient feature in the cluster evolution is their periodic separation and merging as a whole. The periodic morphological change of the clusters is guided by the curved lattice that converges and diverges periodically around the disclinations. This observation suggests that the curvature may be exploited to control the morphology of the moving clusters. For example, in a two-dimensional active matter system realizable by a group of swimming bacteria or other active agents, one may create various geometric structures like Gaussian bumps to control the collective motion [33]. Note that the motions of the clusters in Fig. 3 are collision free for the small size of the clusters.

When the particles occupy the entire spherical lattice, all quasi-uniformly moving along $\hat{e}_\phi$, their collective movement gives rise to multiple bubble structures, as shown in Fig. 4. A frame-by-frame examination shows that, prior to the appearance of these bubbles, local velocity vectors are found to move in and out along multiple directions. The irregularity of these velocity vectors leads to the emergence of void areas embedded in the coarse-grained velocity field. In other words, the bubble structures emerge to avoid singularity in the coarse-grained velocity field. Here, we emphasize that the bubbles are still filled with particles, but the coarse-grained velocity field vanishes therein. Note that in a larger system of $N = 64\,002$, where half of the bonds are occupied by particles, a few coarse-grained velocity vectors are scattered inside some bubbles. It is observed that the bubble size can grow up to about 20 coarse-grained cells from $t = 1$ to $t = 30$. In Figs. 4(a) and 4(b), we also show the collective progression and deformation of the bubbles.

For quasi-uniformly moving particles along $\hat{e}_\theta$ over the entire spherical lattice, each occupying one vertex, we observe vortex structures in addition to the bubble structures, as shown in Fig. 4(b). Vortices are interesting emergent structures in macroscopic hydrodynamic systems. A salient feature of two-dimensional turbulence is the emergence of isolated coherent vortices [38]. Our model allows one to observe the formation of the vortices at the microscopic level. We track the evolution of the coarse-grained velocity vectors and find that the vortices start to form when the group of particles moving quasi-uniformly along $\vec{e}_\theta$ meet those that have passed through the south pole and are moving along $-\vec{e}_\theta$. A typical vortex structure is shown in the dashed ellipse in the last inset in Fig. 4(b). The vortex turns out to be rather robust. It is largely anchored at the same place in the evolving velocity field for a period up to $\Delta t = 10$. It is worth pointing out that the emergence of the nonequilibrium dynamic structures of

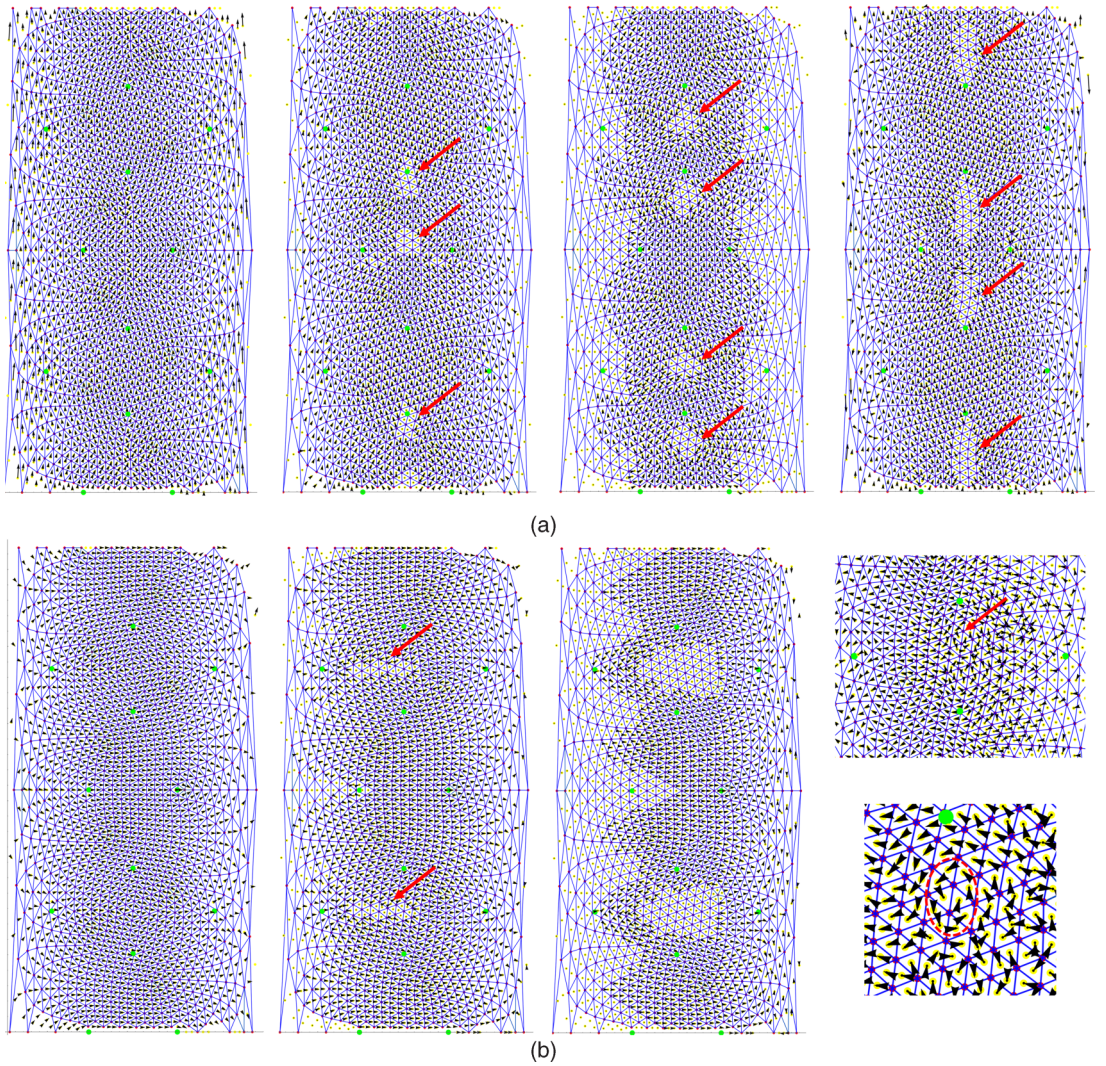


FIG. 4. The bubble and vortex structures developed in the evolution of the coarse-grained velocity field. Each vertex is occupied by a particle in the initial state, and all the particles move quasi-uniformly along (a) $\hat{e}_\phi$ and (b) $\vec{e}_\theta$. (a) The transportation and deformation of the void areas (the bubbles), as indicated by the red arrows. (b) The emergent vortex structure (indicated by the red arrow in the last snapshot whose zoom-in plot is shown below) in addition to the bubbles. The snapshots in (a) and (b) are at (a) $t = 1, 11, 35, 100$ and (b) $t = 1, 16, 45, 278$, respectively. The green dots represent the disclinations. (a) $N = 16002$ and (b) 64002. $N_{cg} = 1002$.

bubbles and vortices results from the bent lattice around the disclinations instead of the disclinations themselves. Figure 4 shows no correlation between the locations of the disclinations and the sites of the bubbles and vortices.

With the accumulation of the collision effect, both the bubble and vortex structures are ultimately destroyed. We track the collision events in the propagation of the particles and plot the frequencies of the binary and triple collisions versus time in Fig. 5 for the case where the particles move quasi-uniformly along $\hat{e}_\phi$. Here the collision frequency refers to the number of the collision events rescaled by the total number of particle movements in a time step. Figure 5 shows that both the binary and triple collision curves exhibit the oscillation behaviors. The period of the oscillation is the same as that of the closed orbit formed by a single particle. Figure 5(a) shows that the binary collision between particles becomes more frequent at a large time scale, and the curve ultimately converges towards an upper bound. In contrast, the oscillation amplitude of the triple collision curve shrinks in time, as shown in Fig. 5(b). With the convergence of both collision curves, the bubble and vortex structures gradually dissolve and the system evolves towards equilibrium.

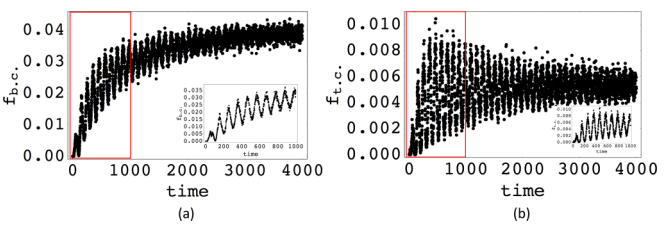


FIG. 5. Plot of the frequencies of the binary and triple collisions versus time. Both curves exhibit the oscillation behaviors. The insets are the zoom-in plots of the curves in the red rectangles. Each vertex is occupied by a particle in the initial state and all the particles move quasi-uniformly along $\hat{e}_\theta$. $N = 16\,002$.

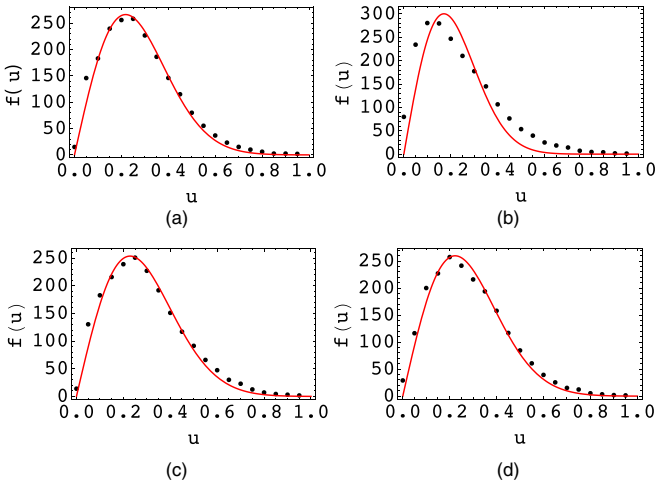


FIG. 6. Roles of the binary and triple collisions on the equilibrium distribution of the tempo-spatially coarse-grained speed. The solid red fitting curves have the common functional form of $f_{fit}(u) = au\exp(-bu^2)$. (a) Both the binary and triple collision rules are shown. (b) The collision free case. (c) Only the binary collision rule. (d) Only the triple collision rule. The time average is over $t \in [100,110]$. The speed is scaled by the maximum coarse-grained speed. Each bond has 50% probability to be occupied by a unit velocity vector in the initial state. The values for the parameters in the fitting function are obtained from the quasi-Newton method. (a) $a = 2014.18$, $b = 10.52$; (b) $a = 2898.48$, $b = 17.1363$; (c) $a = 1827.16$, $b = 9.55697$; (d) $a = 1918.49$. $b = 10.0383$. $N = 64002$. $N_{cg} = 1002$.

Now we analyze the equilibrium property of the spherical lattice gas model. Consider a spherical lattice where each bond in the original lattice has 50% probability to be occupied. It turns out that the influence of the initial state of the system is significantly diminished after tens of time steps. Statistical analysis of the tempospatially coarse-grained velocity field $\vec{u}(\vec{x})$ reveals a stable distribution $f(u)$, as shown in Fig. 6(a). Here $u$ is rescaled by its maximum value. $\vec{u}(\vec{x})$ is defined at the center of each triangular coarse-grained cell, and it is the sum of the velocities of the particles within the coarse-grained cell. $f(u)\Delta u$ is the number of the coarse-grained cells whose associated coarse-grained speed falls between $u$ and $u + \Delta u$. The data in Fig. 6(a) can be well fitted by the function $f_{fit}(u) = au\exp(-bu^2)$. It is recognized as the two-dimensional Maxwell-Boltzmann distribution by expressing $b$ as $b = m/(2k_BT)$, where $k_B$ is the Boltzmann constant, $T$ is the temperature, and $m$ is the total mass of the particles contained in each coarse-grained cell. Since both $m$ and $T$ are linear to the average number of particles $\langle N_{\rm cell}\rangle$ in the coarse-grained cells, $b$ is expected to be independent of the degree of the coarse graining. To check this expectation, we simulate systems with varying $N$. $N = \{25002,36002,49002,64002,81002\}$, and $\langle N_{\rm cell}\rangle = \{36,48,67,88,112\}$, respectively. It is found that $b = 10.81 \pm 0.43$ in all these systems, which is indeed almost an invariant.

To understand the emergent statistical law, we regard each coarse-grained cell as a virtual particle. For convenience in later discussions, the particles in the original spherical lattice are named molecular particles. The movement of the molecular particles into and out of the cells results in the transfer of momentum among neighboring virtual particles. A virtual particle's momentum varies in a "quantum" manner. The minimum momentum change of a virtual particle is the momentum of an individual molecular particle. The effect of the collisions among molecular particles within a virtual particle is to fully randomize the $N_{\rm cell}$ unit velocity vectors $\vec{v}_i$ ($i \in [1,N_{\rm cell}]$) such that these velocity vectors are statistically independent. The velocity of a virtual particle $\vec{u}$ is the sum of the associated molecular particles' velocities:

$$\vec{u} = \sum_{i=1}^{N_{\rm cell}} \vec{v}_i. \tag{2}$$

It is recognized that $\vec{u}$ is essentially the sum of $N_{\rm cell}$ independent and identically distributed random unit vectors $\vec{v}_i$ ($i \in [1,N_{\rm cell}]$). Our problem is therefore mapped to a random walk model defined on a triangular lattice. According to the central limit theorem, the end-to-end distance $r$ of a random walker in a triangular lattice asymptotically conforms to the Rayleigh distribution after a large number of steps [39]

$$p_1(r;N_{\rm cell}) = A_1\frac{r}{N_{\rm cell}}\exp\left[-\frac{r^2}{2r_0^2N_{\rm cell}}\right], \tag{3}$$

where $r_0$ is the lattice spacing of the triangular lattice and $A_1$ is the normalization coefficient. Note that Eq. (3) and $f_{fit}(u)$ in Fig. 6(a) share the same functional form, and both of them correspond to the two-dimensional Maxwell-Boltzmann distribution.

However, we find that $N_{\rm cell}$, the number of particles in the coarse-grained cells, is subject to the Gaussian-type fluctuation, which will be discussed later. This population fluctuation must be taken into account in the random walk model. In other words, the random walk model shall be generalized to allow the fluctuation in the number of steps. The probability density for $N_{\rm cell}$ can be written as

$$p_2(N_{\rm cell}) = A_2\exp\left[-\frac{(N_{\rm cell}-\langle N_{\rm cell}\rangle)^2}{a_2^2}\right]. \tag{4}$$

In the following, we discuss if the population fluctuations in the coarse-grained cells will influence the statistical law governing the speed distribution of the virtual particles. From Eqs. (3) and (4), we have the probability density for $u$:

$$p(u) = \int_0^\infty p_1(u;N_{\rm cell})\times p_2(N_{\rm cell})dN_{\rm cell}, \tag{5}$$

where the integration is over all possible values for $N_{\rm cell}$. We notice that the dominant contribution to the integral is from the domain near $N_{\rm cell} = \langle N_{\rm cell}\rangle$, which is at the peak of the $p_2(N_{\rm cell})$ curve. Eq. (5) can be evaluated by the saddle point method [40]

$$p(u) \approx \frac{Aa_2u}{\langle N_{\rm cell}\rangle}\exp\left[-\frac{u^2}{2u_0^2\langle N_{\rm cell}\rangle}\right], \tag{6}$$

where $A$ is the normalization coefficient and $u_0$ is the magnitude of the molecular velocity vector. By comparing

Eq. (6) with the numerical evaluation of Eq. (5), we find that Eq. (6) is a good approximation even when the standard deviation in $N_{\text{cell}}$ is as large as about 30% around its average value. To conclude, modest population fluctuation in a virtual particle does not change the nature of the statistical law for the distribution of the coarse-grained speed $u$.

In mapping our problem to the generalized random walk model, an important assumption is the collision-driven randomization of the molecular velocity vectors. Now we analyze the specific roles of the binary and triple collisions in achieving the regular statistical distribution. We first remove both types of collisions from our model and examine the consequence. Figure 6(b) shows the distribution of the coarse-grained speed $u$ without any collision. We see that the simulation data are deviated from the two-dimensional Maxwell-Boltzmann distribution. The peak on the curve in Fig. 6(b) is due to the random initial state of the molecular particles. The result presented in Fig. 6(b) indicates that the randomness brought by the initial condition is insufficient to establish a Maxwell-Boltzmann distribution.

To clarify if the solo binary collision suffices to establish the statistical regularity in the speed distribution, we remove the triple collision from the model and keep only the binary collision rule. In Fig. 6(c), we show that the binary collision seems sufficient to destroy the statistical correlation of molecular particles' velocities, and produce the result of the random walk model. We further find that only retaining the triple collision rule in our model also suffices to randomize the velocities, as suggested by the curve in Fig. 6(d). Note that the triple collision typically occurs at a much lower rate than the binary collision. We observe 50% more binary collision events than the triple collision events in the system of about 30 000 molecular particles. These observations suggest that even a relatively rare collision rate between particles can randomize the molecular particles and produce a regular statistical distribution. We also study systems of higher particle densities. It turns out that the collision rate is even lower. In the spherical lattice where 80% of the bonds are occupied and $N = 100\,002$, $f_{b.c.} = 0.06\%$ and $f_{t.c.} = 0.15\%$, which are only 4% and 15% of the corresponding collision frequencies for the case of 50% occupation rate. Even at such a low collision rate, we still observe that the statistics of the coarse-grained speed obeys the Maxwell-Boltzmann distribution.

Collisions between molecular particles are also found to be responsible for the regular statistical distribution of $N_{\text{cell}}$, the number of molecular particles in the coarse-grained cells. Statistical analysis of $N_{\text{cell}}$ in each coarse-grained cell reveals that the distribution of $N_{\text{cell}}$ approaches the Gaussian distribution by adding the collision rules, as illustrated in Fig. 7(a). In Fig. 7(b), we show the linear relation between $N_{\text{cell,max}}$ [the value of $N_{\text{cell}}$ at the peak of the $f(N_{\text{cell}})$ curve] and the total number of molecular particles which is half of $N$. Simulations show that the distribution of the speed $u$ of the virtual particles is well fitted by the Maxwell-Boltzmann distribution when $\langle N_{\text{cell}} \rangle$ is larger than about 40.

Finally, we exploit the fact that the emergent statistical law of the virtual particles' speed is independent of the number of molecular particles $N_{\text{cell}}$ within each virtual particle once $N_{\text{cell}}$ is sufficiently large. The coarse-graining procedure maps the molecular particles into a collection of virtual particles. The

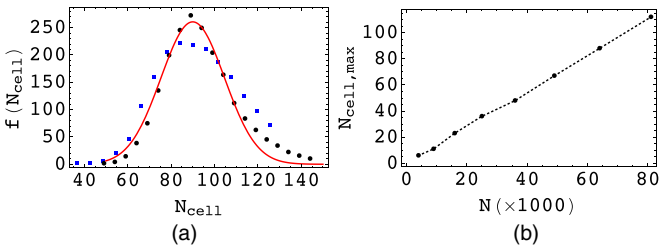


FIG. 7. Analysis of the population fluctuation in the triangular cells of the coarse-grained spherical lattice. (a) The distribution of the number of particles $N_{\text{cell}}$ in each cell. The square blue dots are for the collision free case, and the black dots are for the case with both the binary and triple collision rules. The black dots, especially those near the maximum $N_{\text{cell}}$, are fitted by the Gaussian distribution function. The time average is over $\Delta t = 10$. $N = 64\,002$. $N_{cg} = 1002$. (b) Shows the linear dependence of the maximum $N_{\text{cell}}$ on the number of vertices $N$ in the spherical lattice. The total number of molecular particles is half of $N$. Both the binary and triple collision rules are applied.

velocity of an arbitrary virtual particle labeled $j$ is

$$\vec{u}_j^{(1)} = \sum_{i \in \Omega_j^{(1)}} \vec{v}_i. \tag{7}$$

$\vec{v}_i$ is the velocity of the molecular particle labeled $i$ within the virtual particle $j$. It is a random unit vector whose orientation can take one of the six discrete directions in the triangular lattice with the same probability. The sum in Eq. (7) is over all the molecular particles in the coarse-grained cell $\Omega_j^{(1)}$ that is named as the virtual particle $j$. The superscript "(1)" in $\vec{u}_j^{(1)}$ and $\Omega_j^{(1)}$ denotes the first round coarse-graining procedure from the original molecular particles to the virtual particles. We have shown that the magnitude of the resulting random variable $\vec{u}^{(1)}$ conforms to the two-dimensional Maxwell-Boltzmann distribution. One can perform further coarse graining by classifying all the virtual particles in the newly built coarse-grained cells denoted as $\Omega_k^{(2)}$. Summing over all the virtual particles' velocities in $\Omega_k^{(2)}$ returns a new random variable:

$$\vec{u}_k^{(2)} = \sum_{i \in \Omega_k^{(2)}} \vec{u}_i^{(1)}. \tag{8}$$

The comparison of Eqs. (7) and (8) shows that the magnitude of $\vec{u}^{(2)}$ also obeys the two-dimensional Maxwell-Boltzmann distribution. The coarse-graining procedure can be further extended to higher levels. On the premise that there are sufficient virtual particles in the coarse-grained cells, the statistical law always holds. The transferable statistical law from the original molecular particle system to any coarse-grained system is essentially attributed to the statistical independence of the molecular particles at the very bottom level; no statistical correlation can be built up in the coarse-graining process itself.

## IV. CONCLUSION

In summary, based on the spherical lattice gas automaton with the well-defined propagation and collision rules, we reveal several emergent dynamic structures resulting from the geometric frustration of the collectively moving clusters,

including the periodic global morphological transformations, the bubble and vortex structures embedded in the coarse-grained velocity field. With the accumulation of the collision effect, statistical analysis shows that the coarse-grained speed conforms to the two-dimensional Maxwell-Boltzmann distribution despite the modest population fluctuations. A generalized random walk model is proposed to account for the observed regular statistical behaviors. This work demonstrates the capability of the spherical lattice gas automaton in revealing the nonequilibrium dynamic structures and in producing the statistical law of the real gas. For its simplicity and the capability of simulating physics, the lattice gas automaton model may be generalized to other curved surfaces to explore geometrically driven nonequilibrium physics. Furthermore, considering that the emergent dynamic structures like the bubbles and vortices in our system are largely driven by the disclinations in the lattice, it is of interest to explore the potential collective dynamics regulated by a designed mix of five- and seven-fold disclinations on an almost-planar lattice.

## ACKNOWLEDGMENTS

This work was supported by NSFC Grant No. 16Z103010253, the SJTU startup fund under Grant No. WF220441904, and the award of the Chinese Thousand Talents Program for Distinguished Young Scholars under Grant No. 16Z127060004.

[1] T.-D. Lee and C.-N. Yang, Phys. Rev. **87**, 410 (1952).
[2] R. J. Baxter, *Exactly Solved Models in Statistical Mechanics* (Elsevier, Amsterdam, The Netherlands, 1982).
[3] L. P. Kadanoff, Phys. Today **39**(9), 7 (1986).
[4] L. P. Kadanoff, *From Order to Chaos II: Essays: Critical, Chaotic and Otherwise* (World Scientific, Singapore, 1999).
[5] F. Bagnoli, N. Boccara, and R. Rechtman, Phys. Rev. E **63**, 046116 (2001).
[6] F. Bagnoli, F. Franci, and R. Rechtman, Phys. Rev. E **71**, 046108 (2005).
[7] K. Preston, Jr. and M. J. Duff, *Modern Cellular Automata: Theory and Applications* (Springer Science and Business Media, New York, 2013).
[8] J. Hardy, Y. Pomeau, and O. De Pazzis, J. Math. Phys. **14**, 1746 (1973).
[9] J. Hardy, O. De Pazzis, and Y. Pomeau, Phys. Rev. A **13**, 1949 (1976).
[10] N. Margolus, T. Toffoli, and G. Vichniac, Phys. Rev. Lett. **56**, 1694 (1986).
[11] U. Frisch, B. Hasslacher, and Y. Pomeau, Phys. Rev. Lett. **56**, 1505 (1986).
[12] U. Frisch *et al.*, Complex Systems **1**, 649 (1987).
[13] M. R. Swift, E. Orlandini, W.R. Osborn, and J. M. Yeomans, Phys. Rev. E **54**, 5041 (1996).
[14] J. M. Buick and C. A. Greated, Phys. Rev. E **61**, 5307 (2000).
[15] D. A. Wolf-Gladrow, *Lattice-Gas Cellular Automata and Lattice Boltzmann Models: An Introduction* (Springer, New York, 2004).
[16] S. Wolfram *et al.*, Nature **311**, 419 (1984).
[17] S. Wolfram *et al.*, *Theory and Applications of Cellular Automata*, Vol. 1 (World Scientific, Singapore, 1986).
[18] S. Chen, S. Dawson, G. Doolen, D. Janecky, and A. Lawniczak, Comput. Chem. Eng. **19**, 617 (1995).
[19] J. T. Wootton, Nature **413**, 841 (2001).
[20] A. Deutsch and S. Dormann, *Cellular Automaton Modeling of Biological Pattern Formation: Characterization, Applications, and Analysis* (Springer Science and Business Media, New York, 2007).
[21] R. Kapral and K. Showalter, *Chemical Waves and Patterns*, Vol. 10 (Springer Science and Business Media, New York, 2012).
[22] J. M. Vianney A. Koelman, Phys. Rev. Lett. **64**, 1915 (1990).
[23] P. Manneville, N. Boccara, G. Y. Vichniac, and R. Bidaux, *Cellular Automata and Modeling of Complex Physical Systems: Proceedings of the Winter School, Les Houches, France, February 21–28, 1989*, Vol. 46 (Springer Science and Business Media, New York, 2012).
[24] L. B. Kier, C.-K. Cheng, and B. Testa, J. Theor. Biol. **215**, 415 (2002).
[25] P. Kurka, in *Computational Complexity* (Springer, 2012), pp. 3212–3233.
[26] J. Von Neumann *et al.*, IEEE Transactions on Neural Networks **5**, 3 (1966).
[27] S. Wolfram, Rev. Mod. Phys. **55**, 601 (1983).
[28] G. Y. Vichniac, Physica D **10**, 96 (1984).
[29] T. Toffoli, Physica D **10**, 117 (1984).
[30] R. Cowburn and M. Welland, Science **287**, 1466 (2000).
[31] R. P. Feynman, Int. J. Theor. Phys. **21**, 467 (1982).
[32] F. C. Keber, E. Loiseau, T. Sanchez, S. J. DeCamp, L. Giomi, M. J. Bowick, M. C. Marchetti, Z. Dogic, and A. R. Bausch, Science **345**, 1135 (2014).
[33] M. Marchetti, J. Joanny, S. Ramaswamy, T. Liverpool, J. Prost, M. Rao, and R. A. Simha, Rev. Mod. Phys. **85**, 1143 (2013).
[34] Z. Yao, Soft Matter **12**, 7020 (2016).
[35] P. M. Chaikin and T. C. Lubensky, *Principles of Condensed Matter Physics*, Vol. 1 (Cambridge University Press, Cambridge, England, 2000).
[36] D. Casper and A. Klug, Cold Spring Harbor Symposia on Quantitative Biology **27**, 1 (1962).
[37] D. Struik, *Lectures on Classical Differential Geometry* (Dover, New York, 1988), 2nd ed.
[38] Y. Kaneda and T. Gotoh, *Statistical Theories and Computational Approaches to Turbulence: Modern Perspectives and Applications to Global-Scale Flows* (Springer Science and Business Media, New York, 2013).
[39] H. C. Berg, *Random Walks in Biology* (Princeton University Press, Princeton, NJ, 1993).
[40] G. B. Arfken and H. J. Weber, *Mathematical Methods for Physicists* (AAPT, College Park, MD, 1999).